IOPscience iopscience.iop.org

Home Search Collections Journals About Contact us My IOPscience

Kinetic models for thermal decompositions of amorphous carbon and carbon nitride thin films

This article has been downloaded from IOPscience. Please scroll down to see the full text article.

2003 J. Phys.: Condens. Matter 15 8081

(http://iopscience.iop.org/0953-8984/15/47/011)

View the table of contents for this issue, or go to the journal homepage for more

Download details:
IP Address: 171.66.16.125
The article was downloaded on 19/05/2010 at 17:47

Please note that terms and conditions apply.

INSTITUTE OF PHYSICS PUBLISHING JOURNAL OF PHYSICS: CONDENSED MATTER

J. Phys.: Condens. Matter **15** (2003) 8081–8093 PII: S0953-8984(03)67654-X

Kinetic models for thermal decompositions of amorphous carbon and carbon nitride thin films

Yuan Qing Li and Lihong Zhang[1,2]

Department of Materials Science, National University of Singapore, Singapore 119260

E-mail: LiHong.Zhang@Seagate.com

Received 15 August 2003
Published 14 November 2003
Online at stacks.iop.org/JPhysCM/15/8081

Abstract
Amorphous carbon (a-C) and carbon nitride (a-CN_x) thin films prepared by sputter deposition on thin Corning glass substrates were studied using isothermal thermogravimetry and the differential method. Two typical reaction kinetics, the sigmoid and deceleratory reactions, were observed, which correspond to the films sputtered at higher (0.9–3 mTorr) and lower vacuums (7–16 mTorr), respectively. The structure bonding ratios and activation energies for thermal decompositions, which increased with the kinetic energy of the carbon species during deposition, were used to interpret the observations of reactions. The free bonded and weakly bonded compositions, the amounts of which increased with sputtering pressure, could be active nucleus sites in early reactions determining the reaction kinetics. The films with higher structure bonding ratios showed an induction period for generation of infrequently formed nuclei and had typically sigmoid-type reaction kinetics, while those with large amounts of free and weakly bonded compositions produced large amounts of quickly formed nuclei in early reactions and showed deceleratory reaction kinetics.

1. Introduction

Amorphous carbon (a-C) thin films have many applications due to some of their unique properties such as high hardness, low friction, good wear resistance, surface smoothness, chemical inertness and optical transparency [1–4]. Using reactive deposition, hybrid nitrogenated (a-CN_x) or hydrogenated (a-CH_x) films can be formed, which demonstrate various desirable properties for some applications [5, 6]. The carbon nitride films have attracted especially high interest since Liu and Cohen [7] predicted a β-C_3N_4 phase that is harder than diamond. Most attempts at getting this phase resulted in the growth of amorphous

[1] Author to whom any correspondence should be addressed.
[2] Present address: Seagate Technology International, Singapore Science Park, 118249 Singapore.

0953-8984/03/478081+13$30.00 © 2003 IOP Publishing Ltd Printed in the UK

Table 1. The most important rate equations used in kinetic analysis of solid state reactions [15]. (α: reactant conversion at time t. In this work, it refers to the film reacted at time t.)

	$g(\alpha) = k(t' - t_0) = kt$	$f(\alpha) = (1/k)(\mathrm{d}\alpha/\mathrm{d}t)$
1. Sigmoid α-time		
A2, Avrami–Erofeev	$[-\ln(1-\alpha)]^{1/2}$	$2(1-\alpha)[-\ln(1-\alpha)]^{1/2}$
A3, Avrami–Erofeev	$[-\ln(1-\alpha)]^{1/3}$	$3(1-\alpha)[-\ln(1-\alpha)]^{2/3}$
A4, Avrami–Erofeev	$[-\ln(1-\alpha)]^{1/4}$	$4(1-\alpha)[-\ln(1-\alpha)]^{3/4}$
An, Avrami–Erofeev	$[-\ln(1-\alpha)]^{1/n}$	$n(1-\alpha)[-\ln(1-\alpha)]^{(n-1)/n}$
B1, Prout–Tompkins	$\ln[\alpha/(1-\alpha)]$	$\alpha(1-\alpha)$
2. Deceleratory α-time		
2.1. Geometrical models		
R2, contracting area	$1-(1-\alpha)^{1/2}$	$2(1-\alpha)^{1/2}$
R3, contracting volume	$1-(1-\alpha)^{1/3}$	$3(1-\alpha)^{2/3}$
2.2. Diffusion models		
D1, one-dimensional	α^2	$1/2\alpha$
D2, two-dimensional	$(1-\alpha)\ln(1-\alpha)+\alpha$	$[-\ln(1-\alpha)]^{-1}$
D3, three-dimensional	$[1-(1-\alpha)^{1/3}]^2$	$3/2(1-\alpha)^{2/3}[1-(1-\alpha)^{1/3}]^{-1}$
D4, Ginstling–Brounshtein	$1-(2\alpha/3)-(1-\alpha)^{2/3}$	$3/2[(1-\alpha)^{-1/3}-1]^{-1}$
2.3. 'Order of reaction' models		
F0, zero order	α	1
F1, first order	$-\ln(1-\alpha)$	$1-\alpha$
F2, second order	$[1/(1-\alpha)]-1$	$(1-\alpha)^2$
F3, third order	$[1/(1-\alpha)^2]-1$	$(1-\alpha)^3$

films (a-CN$_x$) which demonstrated improved tribology, electrical and thermal properties and other desirable surface properties compared with the respective a-C films, and have stimulated intensive scientific research in the past few years [8, 9].

One of the most successful applications of the a-C and a-CN$_x$ thin films is as coatings on magnetic hard media and heads protecting against wear and corrosion [10]. The thermal stability of the films required by this application is critically important, mainly because of the high intense local heat generated at a quickly spinning head and disc interface, that can cause film decomposition. This process not only degrades film functions but also generates highly reactive species causing interface smears. Thermal decompositions of a-C and related films are heterogeneous processes that generally happen together with graphitization and loss of structure constituents [11, 12]. This study basically addresses the atomic bonding configuration, bonding intensity and bonding ratio of the structure. All these factors are affected by the kinetic energy of the carbon species while the bonding configuration and intensity can also be adjusted through reactive sputtering as well as plasma energy [13, 14].

Structure thermal decomposition generally initiates either from individual sites (nuclei) or internal surface boundaries. Nucleation is the initial establishment of a new and discrete product particle within the solid reactant. The number of nuclei established and rate of nuclei establishment affect the kinetic reaction processes. Structure defects and weak bonding sites are highly reactive sites for nucleation. Chemical reactions, surface geometry and diffusion are three factors that have been identified as controlling the rates of solid state decompositions, alone or in combination. Some kinetic models, based on quantitative consideration of the three factors mentioned above, have been developed and are listed in table 1 [15].

Thermal stability of hard a-C films has been studied by means of Raman spectroscopy [16], the FTIR approach [17], Auger electron microscopy (AES) [18], thermal desorption [19], stress measurement and friction and wear testing [3]. In general, the films show more graphitic

Raman spectra, an increased friction coefficient, increased index of refraction, reduced stress and increased wear when exposed to high temperatures. The onset of these effects lies typically between 200 and 500 °C. Most thermal stability studies for a-C and related thin films qualitatively addressed the relative stability and dissociation components. The chemical kinetics, rates and mechanisms of the processes, the interpretation of which draws heavily on the interdisciplinary areas between chemistry, physics and branches of engineering, are very important information but given less attention. This study basically investigates the kinetic processes and mechanisms for decompositions of some sputtered a-C and a-CN_x films based on the reaction data acquired from isothermal thermogravimetry (TG) and the corresponding differential thermogravimetry (DTG) techniques. The results are compared and discussed on the basis of film structures affected by the kinetic energies of the carbon species during sputtering.

2. Experimental details

2.1. Film deposition

The a-C and a-CN_x films were deposited at ambient temperature using a DC-magnetron sputtering system (INNOTEC D28) with a base chamber pressure of about 2×10^{-6} Torr, achieved through a cryopump. The films on Corning glass substrates (0.15 mm thick) had a thickness of about 1 μm and were used for TG analysis while those on Si substrates were about 500 Å thick and were used for structure analysis. Both types of substrate had a hand-touchable temperature after sputtering. The glass substrates were pre-heated at 600 °C in air for 1 h and ultrasonically cleaned and dried with nitrogen gas. This treatment is to minimize the substrate weight changes during TG measurements. The total weight loss of thus-treated glass substrate was less than 0.05%, which can be neglected compared to the ∼1% total weight loss of the films. The high purity pyrolytic graphite target (99.999%) that was 60 mm from the substrate was sputter-cleaned prior to each deposition. For the a-C films, four different sputtering pressures of Ar (>99.999%), 0.91, 3.02, 7.05 and 16.12 mTorr, were used, which correspond to the respective Ar flow rates of 19.1, 67.8, 191.6 and 191.6 sccm. The resultant films are denoted as a-C(1), a-C(3), a-C(7) and a-C(16), respectively, using the bracketed numbers to represent the approximate sputtering pressures in millitorrs. For the a-CN_x films, the sputtering was carried out in Ar and N_2 (>99.9995) gas mixtures at 3.02 and 16.12 mTorr at 30% volumetric concentration of N_2. The resultant films are denoted as a-CN_x(3) and a-CN_x(16). Each deposition was carried out at a DC power of 800 W.

2.2. Structure analysis

Fourier transform infrared (FTIR) spectroscopy (Nicolet 760) and Raman spectroscopy (Renishaw 1000) were used for film structure analysis. FTIR spectra were collected using a grazing angle apparatus, while the Raman spectra were obtained using an Ar^+ laser at 514.5 nm. X-ray spectroscopy (XPS, Physical Electronics Quantum 2000) analysis was performed for the binding energies of C 1s, N 1s and the relative atomic ratios of N in the a-CN_x films.

2.3. Thermogravimetry experiment

Isothermal TG measurements were performed using a Du Pont TGA 2950 analyser with a weight sensitivity of 0.1 μg and a temperature accuracy of ±1 °C. A film/substrate sample of 15–20 mg and a constant gas flow rate of 60 cm^3 min^{-1} were used for each measurement. The temperature was raised at 200 °C min^{-1} to the designated temperatures, which were within

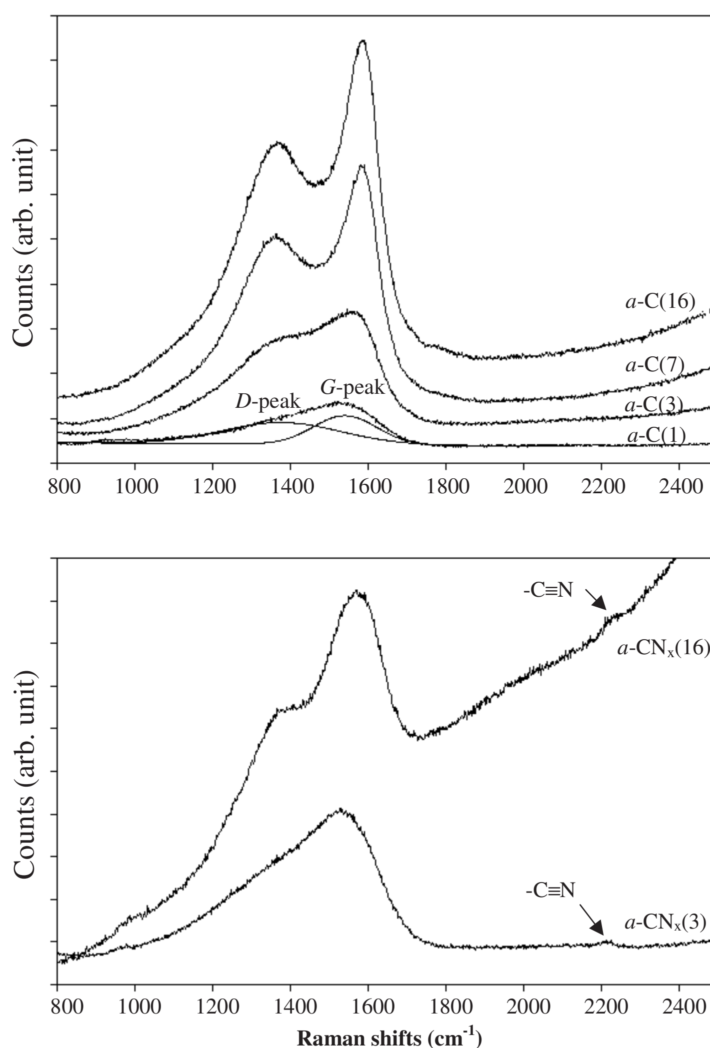

Figure 1. Raman spectroscopy of a-C and a-CN_x films on Si wafer substrates.

350–575 °C for a-C and 450–650 °C for a-CN_x, and then maintained for a period of time. The time duration depends on the amounts of the weight losses of the films at each specific temperature. At 650 °C, the Corning glass substrate might have been softened but no obvious geometry changes were seen, suggesting that the simultaneous heating of the substrate would exert little effect on the reactions of the films.

3. Results and discussion

3.1. Structure analysis of the as-deposited and heated films

Figure 1 shows the Raman spectra of the as-deposited a-C (upper chart) and a-CN_x (lower chart) films. As the sputtering pressure increased, the Raman G-peak moved to higher frequencies while the D-peak and G-peak became better resolved, suggesting that the film graphitization

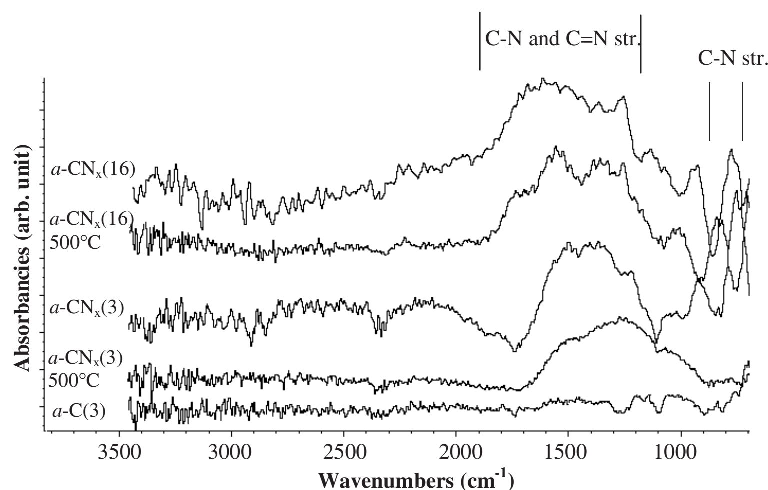

Figure 2. FTIR spectra of the as-deposited and air-heated a-CN_x films in comparison with the as-deposited a-C(3) film.

increased [16]. A small Raman shift at about 2320 cm^{-1} indicates the presence of carbon nitrile (–C≡N) bonds in the a-CN_x films. The enhanced baseline of a-CN_x(16) compared to a-CN_x(3) is due to its photoluminescence property, resulting probably from a highly conjugated structure. The formation of carbon–nitrogen bonds for the a-CN_x films is also clearly revealed by the FTIR spectra shown in figure 2. The presence of carbon–nitrogen single bonds and double bonds can be observed from the IR absorptions between 1100 and 1750 cm^{-1}. From the FTIR and Raman spectra, various carbon–nitrogen bonds observed for the as-deposited a-CN_x films also existed in the structures after heat treatment, as represented by the absorptions of the films at 500 °C in figure 2.

XPS C 1s analysis of the deposited a-C films did not show significant differences in C 1s binding energies. The atomic ratio analysis by means of XPS for the two a-CN_x films showed that the nitrogen concentration was about 14 at.% for the as-deposited films, but reduced to about 9–11% after the films were heated to 600 °C in air. This suggests that nitrogen-rich molecules were evolved during heating, probably due to the presence of some free and weakly bonded carbon–nitrogen compositions in the films.

3.2. Isothermal yield–time and rate curves

The isothermal TG method was used in our previous studies of the sputtered a-C and a-CN_x films to obtain their apparent activation energies (E_a) of thermal decomposition [11, 12]. The E_a values for the a-CN_x films were about 5–40% higher than those for the respective a-C films (87.4–174 kJ mol^{-1}). E_a generally increased with reduction of the sputtering pressures, which increased proportionally with the kinetic energy of the carbon species for deposition. As the reactions proceeded, E_a gradually decreased for the films sputtered at lower pressures (0.9–3 mTorr) but increased for those sputtered at higher pressures (7–16 mTorr). These phenomena have been interpreted on the basis of the differences in structure bonding ratio (the fraction of highly bonded compositions in a structure), which increased as the sputtering pressure reduced, as was revealed by the dynamic TG curves.

Here, we use α to represent the weight loss of the film decomposed at time t. α is also the conversion or yield at that time. Isothermal TG and DTG analysis of the sputtered a-C and

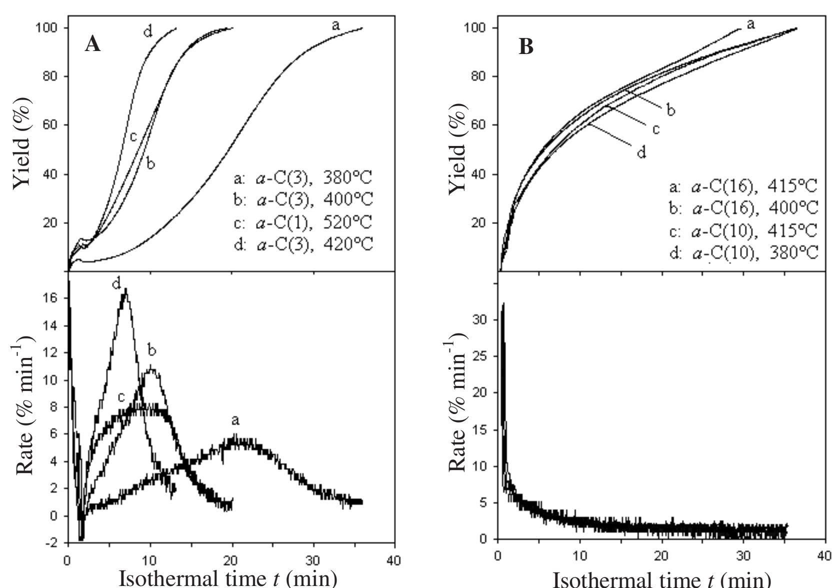

Figure 3. The yield–time and rate–time isothermal TG curves for a-C films. (A) a-C(1) and a-C(3); (B) a-C(7) and a-C(16).

a-CN_x films showed two types of *yield–time* or α–t curve, the sigmoid type and the deceleratory type. The sigmoid yield–time curves were obtained for the films sputtered at lower pressure (a-C(1), a-C(3) and a-CN_x(3)), while for those sputtered at higher pressures (a-C(7), a-C(16) and a-CN_x(16)), deceleratory yield–time curves were obtained. Figures 3 and 4 show the typical yield–time and respective *rate–time* curves or $-\mathrm{d}\alpha/\mathrm{d}t$–$t$ curves for the a-C and a-CN_x films, respectively. The figures show that the yield–time curve types were mainly affected by sputtering pressures rather than by nitrogen incorporation in the films.

From the sigmoid α–t and respective $\mathrm{d}\alpha/\mathrm{d}t$–$t$ curves in figure 3(A) for a-C(1) and a-C(3) and figure 4(A) for a-CN_x(3), it is seen that the decomposition rates accelerated gradually with isothermal time. After passing a maximum (peak) rate, they decelerated initially at almost the same rates as for their accelerating stage, but slowed down obviously as they approached completion, giving $\mathrm{d}\alpha/\mathrm{d}t$–$t$ peaks slightly skewed at late decompositions. For a-C(1), a-C(3) and a-CN_x(3) showing peaks in the $\mathrm{d}\alpha/\mathrm{d}t$–$t$ curves, the time to reach the maximum decomposition rate ($(\mathrm{d}\alpha/\mathrm{d}t)_{\mathrm{max}}$), t_{max}, which is the isothermal time corresponding to the peak value of the $\mathrm{d}\alpha/\mathrm{d}t$–$t$ curves in figures 3(A) and 4(A), decreased with the isothermal temperatures (T_{iso}). This indicates that as T_{iso} increased, the time needed to complete the reactions reduced. Figure 5 shows the typical t_{max}–T_{iso} plots for a-C(1) and a-C(3). From the plots, clear reduction trends of t_{max} with T_{iso} can be observed. The effect of T_{iso} on t_{max} was more significant in the lower T_{iso} region (steeply moving down curves) than in the higher T_{iso} region (gently moving down curves). For the films sputtered at higher pressures (a-C(7), a-C(16) and a-CN_x(16)), $\mathrm{d}\alpha/\mathrm{d}t$ consistently reduced with t; t_{max} was the initial decomposition time.

For a-C(1), a-C(3) and a-CN_x(3), the maximum reaction rate, $(\mathrm{d}\alpha/\mathrm{d}t)_{\mathrm{max}}$ gradually increased with T_{iso}. Meanwhile, the full width at half-maximum (FWHM) of the $\mathrm{d}\alpha/\mathrm{d}t$–$t$ peaks reduced with the peak area which was almost the same at different values of T_{iso}. These phenomena can be clearly seen for a-C(3) in the lower part of figure 3(A). From that part,

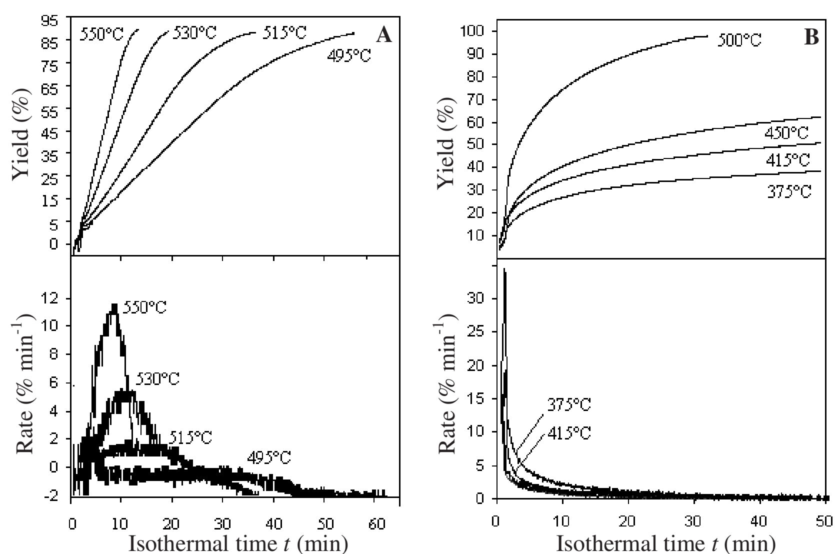

Figure 4. The yield–time and rate–time isothermal TG curves for a-CN_x films. (A) a-CN_x(3); (B) a-CN_x(16).

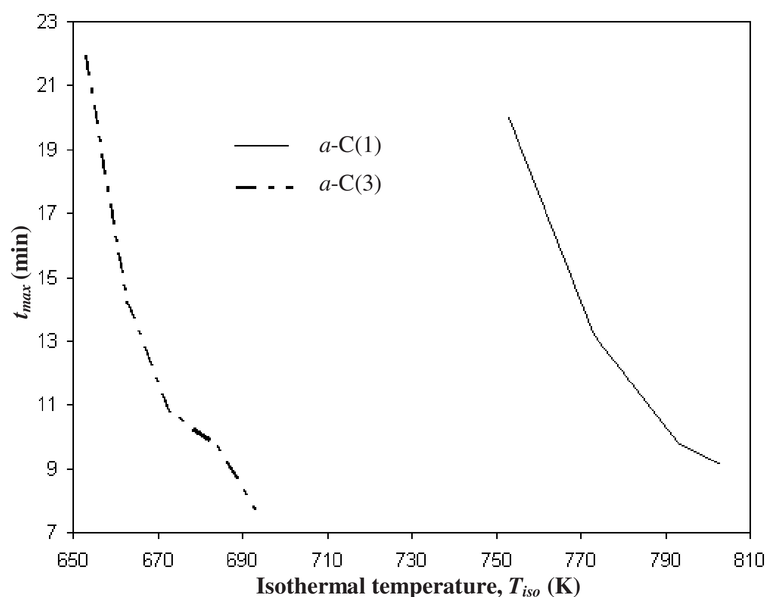

Figure 5. The changes of $t_{\max}$ (time to reach the maximum decomposition rate, $(d\alpha/dt)_{\max}$), with isothermal time for a-C(1) and a-C(3) films.

the FWHM for the film at 380, 400 and 410 °C isothermal temperatures were about 14.7, 7.2 and 7.0 min. Figure 6 shows the changes of FWHM for $d\alpha/dt$–t peaks and $(d\alpha/dt)_{\max}$ with T_{iso} for a-C(1), a-C(3) and a-CN_x(3). Compared to a-C(3), a-C(1) had lower $(d\alpha/dt)_{\max}$ and higher FWHM values at the same T_{iso} (figure 5), indicating that a-C(1) was more stable against thermal decomposition than a-C(3). Compared to a-C(1) and a-C(3), a-CN_x(3) had

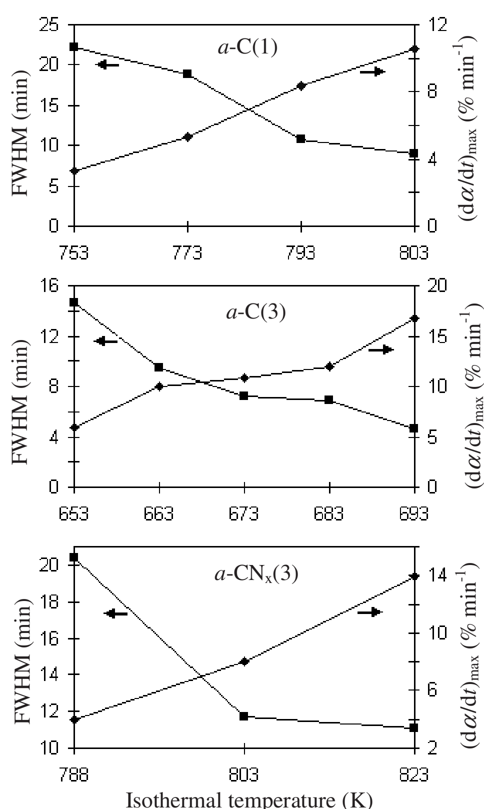

Figure 6. Changes of the FWHM of the $d\alpha/dt$–t peaks and the fastest reaction rate ($(d\alpha/dt)_{max}$) with the isothermal temperature for a-C(1), a-C(3) and a-CN_x(3) films.

an even higher FWHM and lower $(d\alpha/dt)_{max}$ at the same T_{iso}, indicating the significantly increased thermal stability due to incorporation of reactive nitrogen in the film structure. The high thermal stability has been observed from higher E_a values [11, 12].

The sigmoid α–t curves in figures 3(A) and 4(A) for a-C(1), a-C(3) and a-CN_x(3) normally indicate higher activation energies for the initial reactions, which agrees with our data obtained in earlier work [11, 12]. These reactions infrequently formed nuclei due to their higher structure bonding ratio and integration. They accelerated as the stable structures were destroyed. As the reactions approached completion, deceleration was normally observed due to the reduced reactant concentration ($1 - \alpha$, the weight percentage of the films) which was insufficient to maintain a fast reaction. The infrequently formed nuclei could be structure defects or free or weakly bonded sites, the amounts of which were much less significant as compared to those in the films sputtered at higher pressures (a-C(7), a-C(16), a-CN_x(16)). Films having higher sp^3/sp^2 bonding ratios, normally due to the higher impact energy of carbon species during sputtering, have fewer such active sites. Dynamic TG analysis found that the structure bonding ratio of the films decreased with the sputtering pressure due to the decreased kinetic energies of the carbon species for deposition [14]. Therefore, for the films sputtered at lower pressures (a-C(1), a-C(3), a-CN_x(3)), the number of nuclei formed in the early stage could be smaller than that for those sputtered at higher pressures (a-C(7), a-C(16), a-CN_x(16)). However, as the initial stable structure was destabilized due to early decomposition, the reaction would

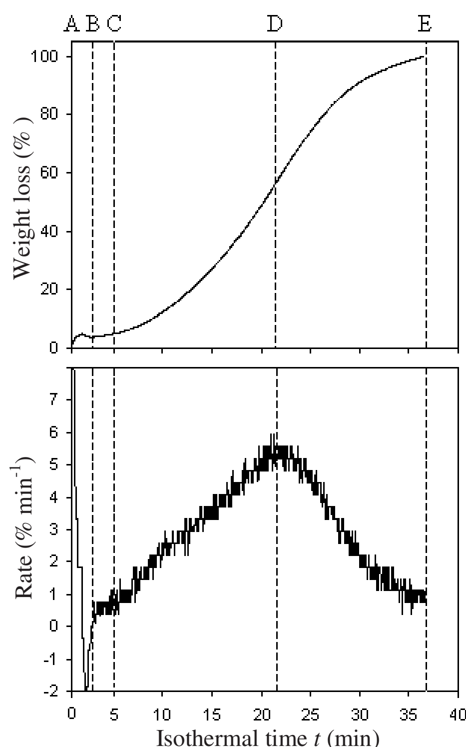

Figure 7. Separation analysis of reaction zones for a typical sigmoid kinetic reaction presented by a-C(3) at 380 °C.

accelerate. Deceleration would appear when the reactant concentration could not maintain a fast reaction rate. This might explain the sigmoid yield–time reaction kinetics for a-C(1), a-C(3) and a-CN_x(3).

For the films sputtered at higher pressures (a-C(7), a-C(16), a-CN_x(16)), larger amounts of free and weakly bonded compositions existed in the structures [15], which were active sites for nucleus formation. In this case, the reactions were fastest in early reaction stages due to the quick formation of a large number of nuclei. With the passage of isothermal time, the number of nuclei reduced through merging and diminishing, causing slowing down of the reactions. This results in the deceleratory yield–time curves (figures 3(B) and 4(B)). These reactions generally have lower activation energies due to easy and quick formation of nuclei, triggering reactions at a fast rate [15], which agrees with the calculated results for activation energies for the a-C and a-CN_x films [11, 12].

The two typical decomposition kinetics for the sputtered a-C and a-CN_x films can be analysed by separating the yield–time curves into sections based on the reaction rates. Figures 7 and 8 show the yield–time and rate–time curves separated into characteristic reaction zones for the sigmoid-type and deceleratory-type reactions obtained at isothermal conditions. The sigmoid yield–time curve (figure 7) presented by a-C(3) at 380 °C could be separated into four reaction zones. The first zone from A to B shows fast weight losses due to the fast evolution of gases in the initial fast heating stage (200 °C min^{-1} to reach the isotherm). The reaction in zone B–C was very slow and is generally regarded as an 'induction' period or incubation period for nucleation. As the isothermal temperature increased, the induction period became

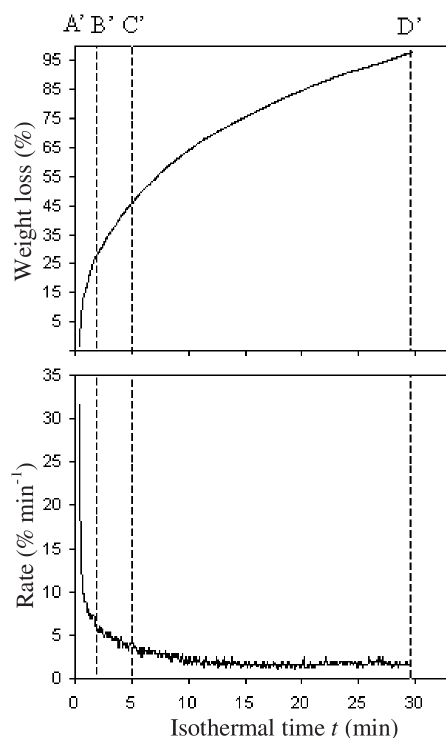

Figure 8. Separation analysis of reaction zones for a typical deceleratory kinetic reaction presented by a-C(16) at 415 °C.

shorter and eventually was too short to be observed in the experimental conditions (figures 3(A) and 4(A)). After the induction, rapid conversion of the acceleratory reaction can be seen, due to the gradual destruction of a highly bonded stable structure, and the reaction went into the third zone B–C. After passing a maximum (peak) rate, the reaction gradually decelerated to form the fourth zone B–D, due to the consumption of reactant (film) that could not sustain a fast reaction. Figure 8 shows the typical deceleratory yield–time and its rate–time curves, using a-C(16) at 415 °C as an example. The reaction could be separated into three typical zones. The first zone from A′ to B′ characterizes the quickest conversion of reactant. This is due to the quick formation of a large number of nuclei in the early reaction. The films sputtered at lower kinetic energy of the carbon species have been characterized by incorporation of a large number of interstitial (free) and weakly bonded compositions [11, 12], which provided typical active sites for structure dissociation. The progress of the reaction gradually caused a reduction in number of some nuclei and the reaction went into a more gentle stage, which was characterized by the second zone B′–C′. In the third zone C′–D′, the reaction rate was almost constant to completion.

3.3. Kinetic reaction models

From the isothermal α–t curves typically shown, figures 3(A) and 4(A), the kinetic equations can be determined by fitting the experimental data with the most commonly used kinetic models. Table 1 lists these models for kinetic analysis of solid state reactions. The results show that the decomposition kinetics of the a-C films at the isothermal temperatures studied could be

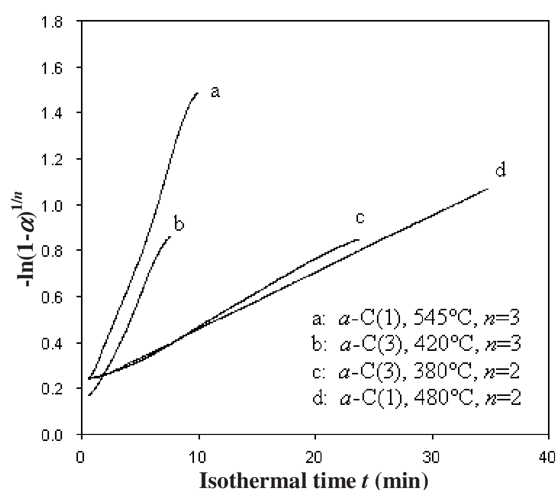

Figure 9. Sigmoid kinetic equations for a-C(1) and a-C(3) at different isothermal temperatures.

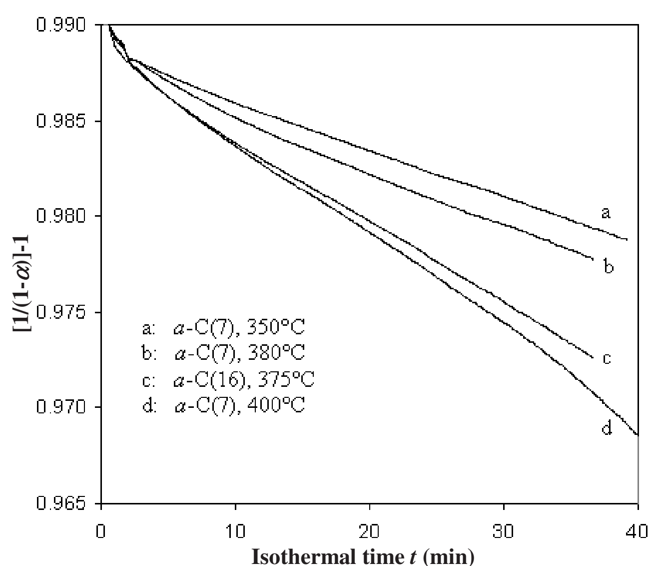

Figure 10. The second-order deceleratory kinetic equations for a-C(7) and a-C(16) at isothermal temperatures from 350 to 400 °C.

best represented by sigmoid type, $g(\alpha) = -\ln(1-\alpha)^{1/n}$, kinetic equations or deceleratory ordered reaction models, where $g(\alpha) = kt$. n is the exponential order, α the percentage of the films decomposed at time t. Figure 9 shows some of the typical $g(\alpha) = kt$ curves for the a-C(1) and a-C(3) studied that showed sigmoid-type reaction kinetics. Figures 10 and 11 show the deceleratory reaction kinetics for a-C(7) and a-C(16) at lower temperatures (350–400 °C) and higher temperatures (>420 °C), respectively. The films a-C(1) and a-C(3) followed $g(\alpha) = [-\ln(1-\alpha)]^{1/n}$ kinetic equations extracted from their sigmoid α–t isothermal curves; the value of n varied from 2 to 3, depending on the film structure and isothermal temperature. From the mathematical expression $[-\ln(1-\alpha)]^{1/n} = kt$, the value of n at fixed

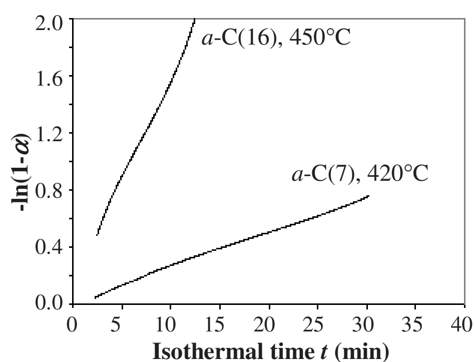

Figure 11. The first-order deceleratory kinetic equations for a-C(7) and a-C(16) at isothermal temperatures from 420 to 450 °C.

α and t reflects a relative rate constant k that is temperature dependent. Generally, a higher n (lower $1/n$) value reflects faster acceleration of a sigmoid-type reaction in the early stage. This may explain the higher n values for a-C(1) and a-C(3) at higher isothermal temperature in figure 9. Films a-C(7) and a-C(16) followed ordered decomposition kinetics with the reaction order changed from 1 to 2, corresponding to $g(\alpha) = -\ln(1-\alpha)$ and $[1/(1-\alpha)]^{-1}$, respectively. The second-order reactions seemed to be followed at lower T_{iso} (350–400 °C, figure 10), but at higher T_{iso} (>400 °C), first-order ones were normally followed (figure 11). Considering that the basic equations for the first-order and second-order reactions are expressed as $d\alpha/dt = -k\alpha$ and $d\alpha/dt = -k\alpha^2$, respectively, the above results for a-C(7) and a-C(16) indicate that the reactions proceeded faster at higher T_{iso}. For all the films, the diffusion-controlled reaction and geometry-controlled reaction models are not suitable for the decompositions of the a-C and related films. This suggests that the films deposited on glass substrates had larger exposure areas for decompositions; therefore, diffusion and geometry do not play significant roles in the kinetic processes of the film decompositions.

For the a-CN_x films, it was found that the sigmoid $g(\alpha) = -[\ln(1-\alpha)]^{1/n}$ kinetic equations with the value of n varying from 8 to 3 could best represent the reaction routes of the films sputtered at lower pressure (1–3 mTorr), while the decompositions for the films sputtered at higher pressures (7–16 mTorr) showing the deceleratory isothermal α–t curves fitted the ordered reaction models best, varying from first order to second order depending mainly on the isothermal temperature. The first-order mechanism was generally observed in high temperature reactions, but in the lower temperature region, the second-order reactions were normally observed. Again, this correlates with faster reactions at higher temperatures. For example, the a-CN_x film prepared in 10% N_2 at 16 mTorr showed a first-order reaction at 375 °C T_{iso} but a second-order one at 425 °C.

4. Conclusions

Amorphous carbon (a-C) and carbon nitride (a-CN_x) thin films were prepared by DC-magnetron sputtering and reactive sputtering on thin Corning glass substrates respectively. Isothermal TG and the DTG methods were successfully applied for studying for thermal decomposition kinetics in air. Two kinds of reaction kinetics, the sigmoid and deceleratory reactions, were observed. The sigmoid reaction kinetics was typically characteristic of the films sputtered at lower pressures (0.9–3 mTorr) or higher kinetic energy of active carbon species

during deposition. This is typically due to their higher structure bonding ratios that had less frequently formed nuclei in early reactions. The acceleration and deceleration of reactions occurred due to gradual destruction of a stable structure and consumed reactant, respectively. The deceleratory reaction kinetics was characteristic for the films sputtered at higher pressures (7–16 mTorr) due to the presence of large amounts of free and weakly bonded compositions that acted as active nuclei in early reactions. The type of the reaction kinetics was little affected by nitrogen incorporation in the films.

The kinetic equations for the films sputtered at higher pressures matched well either that for a first-order reaction or that for a second-order reaction, while the films sputtered at lower pressures followed $[-\ln(1-\alpha)]^{1/n} = kt$ with n varying from 2 to 3 for a-C and 3–8 for a-CN_x.

References

[1] Tsai H-C and Bogy D B 1987 *J. Vac. Sci. Technol.* A **5** 3287
[2] Bhushan B 1999 *Diamond Relat. Mater.* **8** 1985
[3] Robertson J 2002 *Mater. Sci. Eng.* R **37** 129
[4] Tallant D R, Parmeter J E, Siegal M P and Simpson R L 1995 *Diamond Relat. Mater.* **4** 191
[5] Wei B and Komvopoulos K 1997 *J. Tribol.* **119** 823
[6] Strom B D, Bogy D B, Walmsley R G, Brandt J and Bhatia C S 1994 *J. Appl. Phys.* **76** 4651
[7] Liu A Y and Cohen M L 1990 *Phys. Rev.* B **41** 10727
[8] Lin N, Hellgren N, Johansson M P, Hultman L, Erlandsson R and Sundgren J E 2000 *Phys. Rev.* B **61** 4898
[9] Xiao X-C, Jiang W-H, Song L-X, Tian J-F and Hu X-F 1999 *Chem. Phys. Lett.* **310** 240
[10] Han H, Ryan F and McClure M 1999 *Surf. Coat. Technol.* **120/121** 579
[11] Zhang L H, Gong H and Wang J P 2002 *J. Phys.: Condens. Matter* **14** 1697
[12] Zhang L H, Gong H and Wang J P 2002 *J. Appl. Phys.* **92** 2962
[13] Mckenzie D R 1996 *Rep. Prog. Phys.* **59** 1611
[14] Smith D L 1995 *Thin-Film Deposition: Principles and Practice* (New York: McGraw-Hill))
[15] Galwey A K and Brown M E 1999 *Thermal Decomposition of Ionic Solids* (Amsterdam: Elsevier)
[16] Yoshikawa M 1989 *Mater. Sci. Forum* **52/53** 365
[17] Dischler B, Bubenzer A and Koidl P 1983 *Solid State Commun.* **48** 105
[18] Hellgren N, Johansson M P, Broitman E, Hultman L and Sundgren J-E 1999 *Phys. Rev.* B **59** 5162
[19] Xiao X-C, Jiang W-H, Song L X, Hu X F and Lu C W 2000 *Japan. J. Appl. Phys.* **39** L420